Operation-Based Signal-Flow AC Analysis of Switching DC–DC Converters in CCM and DCM

Dongwon Kwon, *Graduate Student Member, IEEE*, and Gabriel A. Rincón-Mora, *Senior Member, IEEE*
Georgia Tech Analog, Power, and Energy IC Research
E-mail: dkwon@ece.gatech.edu, rincon-mora@ece.gatech.edu

***Abstract*—Ensuring stable operation is perhaps one of the most challenging aspects of designing a power-supply circuit because the load is dynamically unpredictable and widely variable. Unfortunately, the nonlinear dynamics of switch-mode converters accentuate these difficulties, especially when considering conventional analytical techniques rely on abstract mathematics to describe ac switching events that convey little operational insight into the circuit. This paper proposes an operation-based signal-flow ac analysis approach that is both sufficiently general to apply to most switched-inductor converters in continuous- and discontinuous-conduction modes (CCM and DCM) and insightful enough to derive directly from the waveforms of the circuit, not from the system of differential equations that govern them. To this end, after presenting the technique, the paper applies it to a relatively simple topology like the buck converter to prove its efficacy and then to a more complex counterpart like the non-inverting buck-boost converter to show the ease with which a more complicated system can be analyzed.**

I. AC Analysis of Switching Converters

Switching dc-dc converters employ negative feedback to regulate the output against variations in load power and (input) line voltage. As a result, understanding the ac characteristics of the system across all possible operating conditions is crucial to ensure the stability of the circuit when subjected to sudden load and/or line changes. Describing these conditional states with equations that reflect the actual operation of the circuit is important to fully comprehend and optimize design tradeoffs. Unfortunately, correlating (insightfully) the nonlinear dynamics of switch-mode circuits is difficult. Therefore, conventional schemes [1-13] first find the operating point through averaging techniques and subsequently linearize the system at that operating point to describe the small-signal operation with equations.

Although the resulting math presents an excellent vehicle to analyze and decipher the stability requirements of the system, the equations remain abstract (with respect to the operation of the circuit). The designer is therefore less able to counter the root-cause factors producing ill-fated effects in the system's response. This paper proposes to bridge this gap by presenting a technique that allows the designer to extract operationally insightful signal-flow graphs (SFGs) directly from inductor-based switching converters operating in both continuous- and discontinuous-conduction modes (CCM and DCM). To this end, for review, Sections II and III of the paper overview the stability objectives and the conventional means of analyzing switching supplies employing negative feedback. Section IV then presents the proposed SFG approach and Section V demonstrates its application to illustrative examples, drawing conclusions in Section VI.

II. Stablity Objective

Negative-feedback loops in switching supplies regulate their outputs by sampling them and using that information to modulate, to whatever extent is necessary, the duty cycle (d_M) of the main switch in the power stage. Determining how a small-signal perturbation propagates through the loop to affect d_M and the output being regulated therefore examines the dynamics of the system, in other words, its ac response [1]. Ensuring the system is stable amounts to preventing signals from phase-shifting (around the loop) to 180° at unity-gain frequency f_{0dB}, which in common terms translates to including phase margin in the response [14]. As a result, understanding what poles and zeros the switch-mode power stage introduces is crucial in establishing stable operating conditions.

This research is supported by Linear Technology Corporation., Milpitas, CA.

III. Conventional Power-Stage AC Models

A. State-Space Averaging (SSA)

Switching converters are comprised of linear sub-circuits designed to operate in switch-mode for the purpose of reducing power losses. In state-space averaging (SSA), state-space-matrix differential equations from each linear sub-circuit are averaged across a switching cycle T_{SW} to eventually describe the small-signal behavior of the system [2-6]. Averaging the response in this manner filters transient effects so the model becomes invalid near the switching frequency f_{SW}. Nevertheless, because developing state-space equations for a linear response is always possible, SSA is general, systematic, and comprehensive. The main challenges here are (i) the frequency-band limitation mentioned, (ii) extracting the ac response of the switching converters from SSA equations is involved, and (iii) although the equations describe the dynamics of the system, they do not often provide physical insight into the origins of the poles and zeros that result.

B. Circuit Averaging

Circuit-averaged models derive linear-equivalent circuits from averaged input-output signals across a nonlinear block, like the switches and diodes of a dc-dc converter [7-8]. In other words, they extract an electrical model comprised of ideal transformers and linearly dependent voltage and current sources from what amounts to SSA-inspired equations. Although this approach presents a circuit, which is operationally more intuitive than SSA equations (with respect to the derived model), it still suffers from the deficiencies attached to SSA because it relies on similarly derived equations.

C. Flow Graph

Flow graphs translate SSA equations into graphical form with nodes and connecting branches [9-13]. Each branch in the graph represents a small-signal transfer function that, when combined with the remaining branches, collectively describe the overall response of the entire loop. Although ascertaining the ac cause-effect relationship between adjacent signals in a flow graph is visually more straightforward than in the previous two approaches, the technique still relies on SSA equations, which means it ultimately suffers from the same shortcomings. Additionally, flow graphs in the literature are invalid in DCM, and developing DCM models from conventional equation-based means is complicated.

IV. Proposed Operation-Based Signal-Flow Graph

A. Approach

The proposed signal-flow graph (SFG) recognizes the ease with which flow graphs in [9-13] convey information so it adopts a similar display format but derives its "branching" relationships directly from the operation of the circuit, ascribing more insight into the graph. The idea is for SFGs to literally trace ac-signal paths across a switching converter circuit and replace its constituent circuit blocks (e.g., switched inductors, capacitors, etc.) with their corresponding branching equivalents. Since the approach extracts the SFG from circuit-produced waveforms, not from the complex matrix of state-space differential equations, the proposed method is able to develop a unified SFG that applies to both CCM and DCM operation, allowing designers to more easily grasp and design for the stability requirements of switching converters across operation modes. As in [1-13], though, the proposed approach still "averages" the response across a switching cycle so its results remain valid for frequencies that fall below f_{SW}.

In the paper, (i) lower case variables with upper case subscripts (e.g., i_L) include dc and ac components, (ii) all upper case variables (e.g., I_L)

describe dc signals only, (iii) all lower case variables (e.g., i_l) represent ac signals only, and (iv) lower case variables that include "(avg)" in their subscripts (e.g., $i_{l(avg)}$) refer to per-cycle averages of ac signals.

B. SFGs for Impedances

The foregoing SFG traces how small-signal variations propagate across a circuit and shows how circuit elements affect them. An impedance Z, for example, converts the voltage across its terminals v_Z into a current i_Z that is equal to v_Z/Z so its SFG representation (Fig. 1a) depicts ac signals v_z and i_z and connects them with a 1/Z branch. Conversely, Z transforms i_z to v_z with a Z branch (i.e., $v_z = i_zZ$) (Fig. 1a). This means resistors (R), inductors (L), and capacitors (C) similarly relate currents and voltages with R, sL, and 1/sC branches, respectively (Fig. 1b-d).

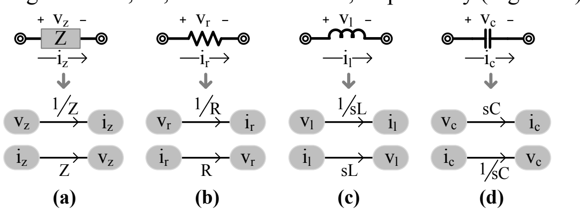

Fig. 1. SFG equivalents for impedances and related passives.

C. Physical Interpretation of Poles and Zeros

Since the purpose of the graph is to illustrate how a circuit affects the ac-signal response, understanding how poles and zeros arise is important. From control theory, the effect of a pole or a zero is to attenuate or intensify signal strength at 20dB per decade of frequency. Said differently, poles *draw* energy away from a passing signal while zeros *contribute* energy [14]. Consider, for example, how shunting capacitor C_O in Fig. 2a shunts the current (energy) away from resistor R_O to ground as the impedance across C_O decreases with increasing frequencies. The net effect is for v_O to decrease with frequency at –20dB per decade, which amounts to the effect of a pole.

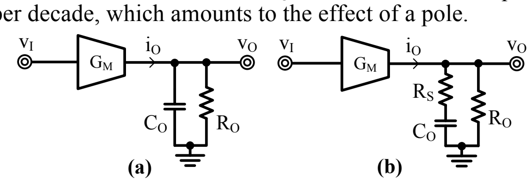

Fig. 2. Shunting capacitors produce poles and zeros.

Similarly, C_O in Fig. 2b also draws current (energy) away from R_O, producing the effect of a pole. The difference here is the series resistor R_S ultimately limits the current to v_O/R_S, when C_O becomes, for all practical purposes, an ac short. In other words, C_O no longer has a shunting effect on v_O when $1/sC_O$ drops below R_S, which equates to saying R_S and C_O cancel the pole R_S, R_O, and C_O produced in the first place. Control theory dictates a zero cancels a pole so series resistor R_S in Fig. 2b produces a zero.

More generically, zeros feed additional energy to a passing signal, or in the case of Fig. 2b, stop a pole from subtracting energy. From a circuit perspective, paths that feed-forward current (e.g., i_{FF}) around an existing (main) path and its related current (e.g., i_O'), as feed-forward transconductors G_{FF}'s exemplify in Fig. 3, can add sufficient energy to R_O to increase $|v_O|$, producing the effect of a zero (when i_{FF} exceeds i_O'). Note, however, Fig. 3b's $-G_{FF}$ inverts the signal with respect to the main path (i.e., i_{FF} is out of phase with i_O'), which is detrimental when considering negative feedback relies on no inversion ($+G_M$) across the block. The out-of-phase, feed-forward path in Fig. 3b therefore contributes a signal-strength intensifying zero that subtracts phase, which control theory calls a right-half-plane (RHP) zero. On the other hand, the in-phase, feed-forward path in Fig. 3a introduces a more benign left-half-plane (LHP) zero.

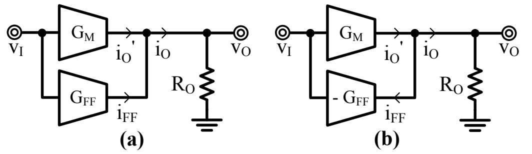

Fig. 3. Feed-forward paths produce (a) LHP and (b) RHP zeros.

D. SFG for a Switched Inductor

CCM and DCM Operation: Switched inductors in dc-dc converters transfer energy from a source to one or several outputs in alternating energizing and de-energizing cycles. Inductor current i_L (Fig. 4), as a result, increases when applying a positive energizing voltage V_{EN} across L_O at a rate of V_{EN}/L_O and decreases when applying a negative de-energizing voltage V_{DE} at V_{DE}/L_O. CCM refers to L_O conducting current continuously across its switching period T_{SW} (Fig. 4a), which means T_{SW} is literally L_O's conduction time t_C. DCM, in contrast, implies L_O ceases to conduct current before T_{SW} ends (Fig. 4b), which corresponds to L_O fully exhausting its stored energy before reaching the end of L_O's switching cycle. In other words, t_C is a fraction of T_{SW}.

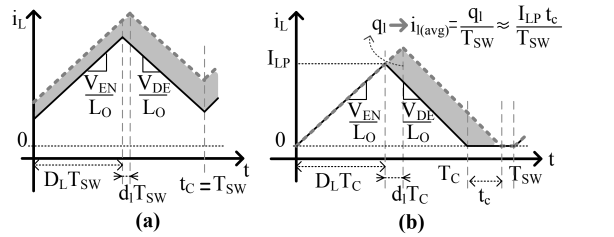

Fig. 4. (a) CCM and (b) DCM waveforms of a switched inductor L_O.

Equivalent SFG: Since t_C in CCM is T_{SW}, small signal t_c is zero and small positive increments in inductor duty cycle d_L increase and decrease energizing and de-energizing times, respectively, by d_lT_{SW}. As a result, there is remnant energy in L_O at the end of T_{SW} that increases average (per cycle) inductor voltage $v_{l(avg)}$:

$$v_{l(avg)} = d_l\left(V_{EN} - V_{DE}\right), \tag{1}$$

causing average inductor current $i_{l(avg)}$ to subsequently increase:

$$i_{l(avg)} = \frac{v_{l(avg)}}{sL_O}. \tag{2}$$

Hence, in CCM, as shown in Fig. 5a, d_l controls $i_{l(avg)}$ by modulating the voltage $v_{l(avg)}$. Since $i_{l(avg)}$ decreases linearly with frequency because of inductor impedance sL_O, this signal path introduces a pole.

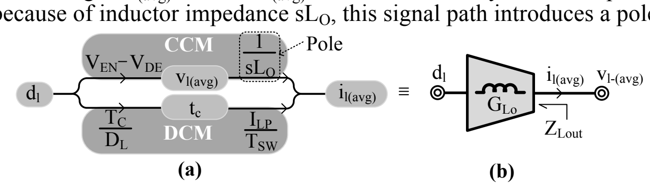

Fig. 5. (a) Partial SFG for a switched inductor L_O and (b) its equivalent duty-cycle controlled current source representation.

On the other hand, because t_C in DCM is a fraction of T_{SW}, both energizing and de-energizing times increase (by d_lT_C and t_c) with an incremental increase in d_L (Fig. 4b). Fully depleting L_O's stored energy at the end of t_C means $v_{l(avg)}$ remains unchanged (at zero). Conduction time t_C, however, is no longer constant (at T_{SW}) and changes with d_l:

$$t_c = d_l\left(\frac{T_C}{D_L}\right), \tag{3}$$

setting how much charge (q_l) L_O transfers per T_{SW} (i.e., $i_{l(avg)}$):

$$i_{l(avg)} = \frac{q_l}{T_{SW}} = t_c\left(\frac{I_{LP}}{T_{SW}}\right), \tag{4}$$

where I_{LP} is i_L's peak ripple current (from Fig. 4b). Therefore, in DCM (Fig. 5a), d_l controls $i_{l(avg)}$ by modulating t_c. Notice L_O in DCM no longer generates a pole, as conventional analyses corroborate [3-7]. Also note that $v_{l(avg)}$ being zero in DCM nulls the effects of the CCM path, just as t_c being zero in CCM nulls those of the DCM counterpart.

Although the transfer function differs, L_O is ultimately a duty-cycle controlled current source in both CCM and DCM (Fig. 5b). As in all practical current sources, the switched inductor's output impedance Z_{Lout} is not infinitely large so $i_{l(avg)}$ changes with variations in L_O's output terminal $v_{l-(avg)}$ (i.e., loading effect). Hence, $i_{l(avg)}$ can be set by super imposing two signal-paths from the input (d_l) and output ($v_{l-(avg)}$) terminal voltage:

$$i_{l(avg)} = d_lG_{Lo} + \frac{-v_{l-(avg)}}{Z_{Lout}}. \tag{5}$$

Impedance Z_{Lout} reduces to sL_O in CCM because L_O always conducts current, which means L_O's complete SFG equivalent in CCM (Fig. 6) not only connects d_l to $v_{l+(avg)}$ with $V_{EN}–V_{DE}$ and $v_{l+(avg)}$ to $i_{l(avg)}$ with $1/sL_O$ branches but also $v_{l-(avg)}$ to $i_{l(avg)}$ via a $-1/sL_O$ branch.

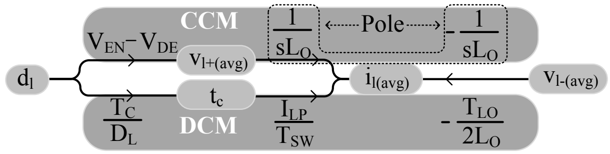

Fig. 6. Complete SFG for switched inductor L_O.

However, impedance Z_{Lout} is no longer sL_O in DCM, because i_L is discontinuous. Applying a test voltage $v_{T(avg)}$ to the output as in Fig. 7, and deriving the resulting charge-per-cycle current $i_{T(avg)}$ reveals

$$Z_{Lout}=\frac{v_{T(avg)}}{i_{T(avg)}}=\frac{2L_O}{T_{LO}}, \tag{6}$$

where T_{LO}, a fraction of T_{SW}, is the amount of the time that L_O conducts because of the output voltage of L_O. Hence, L_O's SFG not only connects d_l and t_c with T_C/D_L and t_c to $i_{l(avg)}$ with I_{LP}/T_{SW} branches in DCM but also $v_{l-(avg)}$ to $i_{l(avg)}$ with $-T_C/2L_O$ branch (Fig. 6).

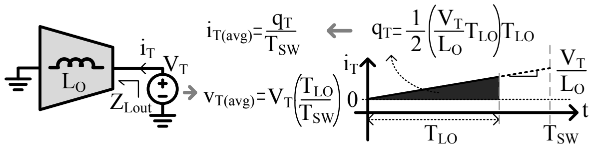

Fig. 7. Deriving switched inductor L_O's output impedance in DCM.

E. SFG for Output Conduction

Not all switching converters connect L_O directly to output v_O, which means i_L is not necessarily equal to output current i_O. In the case i_L is not i_O, an output conducting diode D_O systematically channels i_L to v_O only during output conduction time t_O, as shown in Fig. 8a, which is a fraction of L_O's conduction time t_C. Hence, $i_{o(avg)}$ in CCM is

$$i_{o(avg)}=i_{l(avg)}\left(\frac{T_O}{T_C}\right). \tag{7}$$

In DCM, however, when the duty cycle is increased by d_l, all the increased charge (energy) in L_O (q_l in Fig. 4b) flows to the output (q_o in Fig. 8b), as shown in Fig.8b, so $i_{o(avg)}$ is $i_{l(avg)}$. The SFG equivalent for D_O (shown in Fig. 8c) therefore relates $i_{l(avg)}$ and $i_{o(avg)}$ with T_O/T_C and 1 branches in CCM and DCM, respectively.

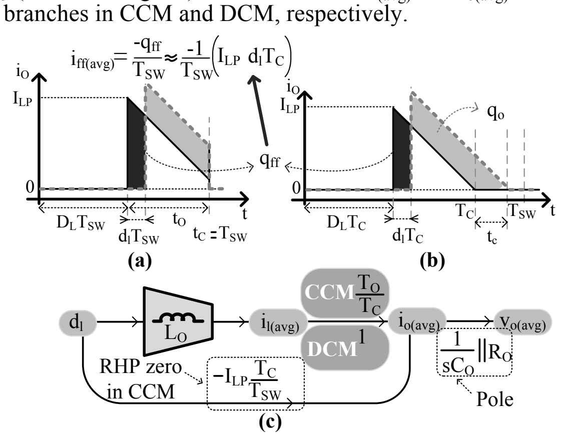

Fig. 8. (a) CCM and (b) DCM output current i_O and (c) its SFG equivalent.

As shown in Fig. 8a-b, an incremental increase in duty cycle d_L not only (i) extends the energizing time by d_lT_C and increases, as a result, $i_{l(avg)}$ and $i_{o(avg)}$, but also (ii) decreases t_O by the same factor, effectively decreasing $i_{o(avg)}$ in consequence. Because D_O's feed-forward impact on $i_{o(avg)}$ (ii) produces an opposing effect with respect to $i_{l(avg)}$'s (i), this out-of-phase feed-forward path produces a RHP zero (z_{RHP}). In this case, out-of-phase, feed-forward current $i_{ff(avg)}$ is the charge *not* transferred (q_{ff} in Fig. 8a-b) over T_{SW}, relating d_l and $i_{o(avg)}$ via $i_{ff(avg)}$ in the SFG with a $-I_{LP}T_C/T_{SW}$ branch

$$i_{ff(avg)}=-d_l\left(\frac{I_{LP}T_C}{T_{SW}}\right). \tag{8}$$

The resulting z_{RHP} occurs at the frequency when $i_{ff(avg)}$ begins to exceed $i_{l(avg)}$'s portion of $i_{o(avg)}$ (i_O' in Fig. 3b or $i_{o(avg)}'$). Since t_C equals T_{SW} in CCM, T_C/T_{SW} reduces to 1, $i_{ff(avg)}$ to d_lI_{LP}, and z_{RHP} to the constant contained below:

$$i_{o(avg)}'\Big|_{z_{RHP(CCM)}=\left(\frac{V_{EN}-V_{DE}}{2\pi I_{LP}L_O}\right)\left(\frac{T_O}{T_C}\right)}=d_l\left(\frac{V_{EN}-V_{DE}}{sL_O}\right)\left(\frac{T_O}{T_C}\right)\equiv i_{ff(avg)}=d_lI_{LP}. \tag{9}$$

Note the loading effect of the switched inductor is neglected here because Z_{Lout} near z_{RHP} (i.e., at high frequencies) is typically much greater than the loading impedance.

In DCM, as shown in the SFG illustrated in Fig. 8c, $i_{o(avg)}'$ is higher to the point it always exceeds $i_{ff(avg)}$:

$$i_{o(avg)}'=d_l\left(\frac{T_C}{D_L}\right)\left(\frac{I_{LP}}{T_{SW}}\right)>i_{ff(avg)}=d_lI_{LP}\left(\frac{T_C}{T_{SW}}\right). \tag{10}$$

Since $i_{ff(avg)}$ cannot invert $i_{o(avg)}$, the RHP zero present in CCM disappears in DCM, as corroborated by [3-7]. In the end, $i_{o(avg)}$ flows to v_O so output capacitor C_O and loading output resistor R_O ultimately convert $i_{o(avg)}$ to $v_{o(avg)}$ with a $(1/sC_O)||R_O$ branch.

V. VALIDATION

A. Buck Converter

The switched inductor (L_O) in a buck converter (Fig. 9a) transfers energy from input V_{IN} to output v_O. Operationally, L_O energizes from V_{IN} to v_O and de-energizes from v_O to ground so V_{EN} is $V_{IN}-V_O$ and V_{DE} is $0-V_O$, as shown in Fig. 9b's SFG when relating d_l and $v_{l+(avg)}$. Since L_O is directly connected to v_O, output conduction time t_O equals L_O's conduction time t_C and $i_{l(avg)}$ is $i_{o(avg)}$. As a result, $v_{o(avg)}$ and $v_{l-(avg)}$ connect via a T_C/T_{SW} branch, $v_{l-(avg)}$ and $i_{l(avg)}$ with $-1/sL_O$ and $-T_C/2L_O$ branches for CCM and DCM, respectively, and $i_{l(avg)}$ and $v_{o(avg)}$ with a $1/sC_O||R_O$ branch, as shown collectively in Fig. 9b.

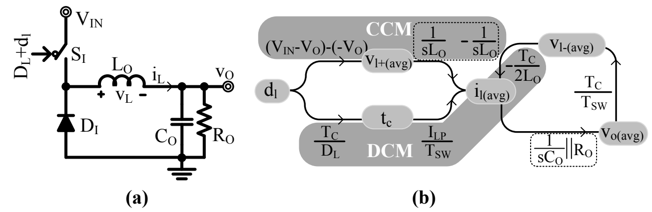

Fig. 9. Buck converter's (a) circuit and (b) equivalent SFG.

Before deriving $v_{o(avg)}/d_l$ to ascertain the stability of the system, note a negative-feedback control loop (that is not shown in Fig. 9a) senses and amplifies $v_{o(avg)}$ to set d_l. As a result, at high frequency, L_O's input (d_l) will dominantly set $i_{l(avg)}$, and the SFG path carrying $v_{l-(avg)}$ signal can be neglected. Hence, in CCM, $v_{o(avg)}/d_l$ can be simplified to the product of the CCM branches that connect $v_{o(avg)}$ and d_l in Fig. 9b's SFG:

$$\left.\frac{v_{o(avg)}}{d_l}\right|_{CCM}\approx V_{IN}\left(\frac{1}{sL_O}\right)\left(\frac{1}{sC_O}\parallel R_O\right)=\frac{V_{IN}R_O}{sL_O\left(1+sC_O\right)}, \tag{11}$$

which means the buck converter's power stage introduces a complex-conjugate pair of poles approximately at $1/2\pi(L_OC_O)^{1/2}$. In DCM, on the other hand, $v_{o(avg)}/d_l$ reduces to

$$\left.\frac{v_{o(avg)}}{d_l}\right|_{DCM}\approx\left(\frac{T_C}{D_L}\right)\left(\frac{I_{LP}}{T_{SW}}\right)\left(\frac{1}{sC_O}\parallel R_O\right)=\left(\frac{2V_O}{D_L}\right)\frac{1}{\left(1+sR_OC_O\right)}, \tag{12}$$

because $I_{LP}T_C/2$ is the charge flowed to the output during T_{SW}, and

$$\left(\frac{I_{LP}T_C}{2}\right)\left(\frac{1}{T_{SW}}\right)=I_O=\frac{V_O}{R}, \tag{13}$$

the power stage only introduces one pole approximately at $1/2\pi R_OC_O$. Had the path carrying $v_{l-(avg)}$ not been neglected, the SFG would have produced the following more accurate results:

$$\left.\frac{v_{o(avg)}}{d_l}\right|_{CCM}=\frac{V_{IN}}{1+s\left(\frac{L_O}{R_O}\right)+s^2\left(L_OC_O\right)} \tag{14}$$

and

$$\left.\frac{v_{o(avg)}}{d_l}\right|_{DCM}=\left(\frac{2V_O}{D_L}\right)\frac{1}{\left(\frac{2V_{IN}-V_O}{V_{IN}-V_O}\right)+s\left(R_OC_O\right)}, \tag{15}$$

which corroborate the SSA relationships derived in [6]. The SPICE-generated frequency-response plots shown in Fig. 10a-b further illustrate and corroborate these results.

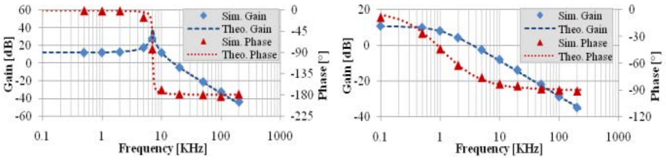

(a) (b)

Fig. 10. Comparison of AC response plots from the proposed SFG analysis to the simulation results of the buck converter in (a) CCM and (b) DCM.

B. *Non-Inverting Buck-Boost Converter*

Like in buck converters, a non-inverting buck-boost converter transfers energy from input V_{IN} to output v_O (Fig. 11a). Switched inductor L_O in this case energizes from V_{IN} to ground and de-energizes from ground to v_O so V_{EN} is V_{IN} and V_{DE} is $-V_O$ and the corresponding SFG (Fig. 11b) connects d_I and $v_{I+(avg)}$ with a V_{IN}+V_O branch. Unlike the buck converter, diode D_O only connects L_O to v_O during the de-energizing cycle, which means output conduction time t_O is a fraction of L_O's conduction time t_C (i.e., $T_O=(1-D_L)T_C$), and consequently, $i_{I(avg)}$ relates to $i_{o(avg)}$ through (1-D_L) branch in CCM (Fig. 11b). On the other hand, in DCM, all the increased charge in L_O due to the increased d_I is transferred to the output, and therefore, $i_{I(avg)}$ equals to $i_{o(avg)}$. Although the increased d_I increases $i_{o(avg)}$, it also shortens the t_O and decreases the $i_{o(avg)}$. Hence, an out-of-phase signal path, which induces a RHP zero in CCM, from d_I to $i_{o(avg)}$ with connecting branch $-I_{LP}T_C/T_{SW}$ is produced (Fig. 11b).

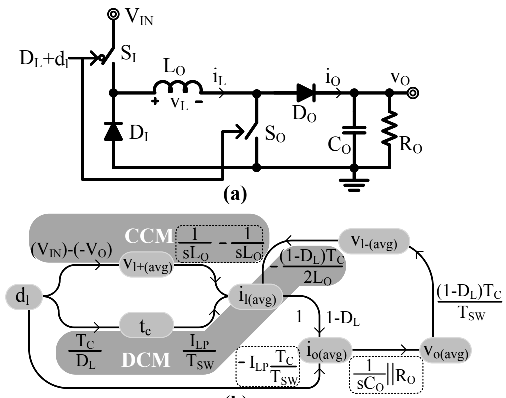

(b)

Fig. 11. Non-inverting buck-boost's (a) circuit and (b) equivalent SFG.

Like in buck converters, the input (d_I) of L_O carries considerably greater feedback energy than $v_{I-(avg)}$ so the SFG path attached to $v_{I-(avg)}$ can be neglected at high frequency. As a result, neglecting the effects of the $-I_{LP}T_C/T_{SW}$ feed-forward path, $v_{o(avg)}'/d_I$ in CCM reduces to the product of the CCM branches that connect $v_{o(avg)}$ to d_I:

$$\left.\frac{v_{o(avg)}'}{d_I}\right|_{CCM} \approx (V_{IN}+V_O)\left(\frac{1}{sL_O}\right)(1-D_L)\left(\frac{1}{sC_O}\parallel R_O\right), \tag{16}$$

which again approximately estimates a complex-conjugate pair of poles at $1/2\pi(L_OC_O)^{1/2}$. When the-out-of-phase feed-forward current d_II_{LP} exceeds its counterpart, $v_{o(avg)}$ reverses polarity and a RHP zero asserts its effects:

$$d_I(V_{IN}+V_O)\left(\frac{1}{sL_O}\right)(1-D_L)\Bigg|_{z_{RHP(CCM)}\approx\frac{(V_{IN}+V_O)(1-D_L)}{2\pi I_{LP}L_O}} \equiv d_II_{LP}\quad, \tag{17}$$

which means

$$\left.\frac{v_{o(avg)}}{d_I}\right|_{CCM} \approx (V_{IN}+V_O)\left(\frac{1}{sL_O}\right)(1-D_L)\left(\frac{1}{sC_O}\parallel R_O\right)\left(1-\frac{s}{z_{RHP(CCM)}}\right). \tag{18}$$

Not neglecting the path containing $v_{I-(avg)}$ and replacing I_{LP} and V_{IN} with their equivalents (i.e., $I_{LP}\approx I_L=(1-D_L)I_O$, $V_{IN}=(1-D_L)V_O/D_L$), assuming small inductor ripple current as in [6], produce the following more accurate relationship:

$$\left.\frac{v_{o(avg)}}{d_I}\right|_{CCM} = \left[\frac{V_O}{D_L(1-D_L)}\right]\frac{1-s\left(\frac{D_LL_O}{(1-D_L)^2R_O}\right)}{1+s\left(\frac{L_O}{(1-D_L)^2R_O}\right)+s^2\left(\frac{L_OC_O}{(1-D_L)^2}\right)}. \tag{19}$$

In DCM, not only does $1/sL_O$ disappears from d_I to $i_{I(avg)}$ but $i_{I(avg)}$ is also large enough to never allow its feed-forward counterpart to overwhelm it, which means the RHP zero present in CCM is absent in DCM. The ac response therefore reduces to

$$\left.\frac{v_{o(avg)}}{d_I}\right|_{DCM} = \left(\frac{V_O}{D_L}\right)\frac{1}{1+s\left(\frac{R_OC_O}{2}\right)}, \tag{20}$$

which only has one pole at $1/\pi R_OC_O$. These results correspond to those derived from SSA equations in [6] and emulate the SPICE results shown in Fig. 12a-b.

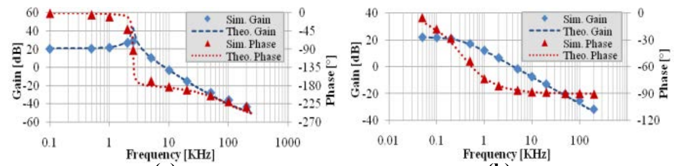

(a) (b)

Fig. 12. Comparison of AC responses from the proposed SFG analysis to the simulation results of the non-inverting buck-boost converter in (a) CCM and (b) DCM.

VI. CONCLUSIONS

The proposed operation-based signal-flow graph (SFG) not only easily conveys ac information graphically but also derives its connecting relationships directly from the operation of the circuit, from its defining waveforms, ascribing more insightful information into the graph and applying to both continuous- and discontinuous-conduction modes (CCM and DCM). Extracting the loop gain and presence of poles and zeros in complicated switch-mode circuits in this way allows the designer to more easily examine and optimize the frequency response of otherwise considerably complicated and abstract state-space-averaged equations. The ultimate and perhaps more important benefit, however, is the ability to design a higher performance (e.g., higher bandwidth, higher accuracy, etc.) switching supply, which is increasingly critical and difficult in state-of-the-art applications like wireless portable devices and energy harvesting ICs.

REFERENCES

[1] G. Wester and R. Middlebrook, "Low-Frequency Characterization of Switched DC-DC Converters," *IEEE Trans. Aerosp. Electron. Syst.,* v. AES-9, n. 3, pp. 376-385, May 1973.

[2] R. Middlebrook and S. Ćuk, "A General Unified Approach to Modelling Switching-Converter Power Stages," *International Journal of Electronics*, v. 42, n. 6, pp. 521-550, 1977.

[3] D. Maksimović and S. Ćuk, "A Unified Analysis of PWM Converters in Discontinuous Modes," *IEEE Trans. Power Electron.,* v. 6, n. 3, pp. 476-490, July 1991.

[4] J. Sun, M. Greuel, P. Krein and R. Bass, "Modeling of PWM Converters in Discontinuous Conduction Mode – A Reexamination," in Proc. IEEE PESC '98, pp. 615-622, June 1998.

[5] J. Sun, D. Mitchell, M. Greuel, P. Krein, and R. Bass, "Averaged Modeling of PWM Converters Operating in Discontinuous Conduction Mode," *IEEE Trans. Power Electron.,* v. 16, n. 4, pp. 482-492, July 2001.

[6] R. Erickson and D. Maksimović, *Fundamentals of Power Electronics 2'nd Ed.,* New York: Springer Science+Business Media, LLC, 2001.

[7] V. Vorpérian, "Simplified Analysis of PWM Converters Using Model of PWM Switch Part I & II," *IEEE Trans. Aerosp. Electron. Syst.,* v. 26, n. 3, pp. 490-505, May 1990.

[8] S. Ben-Yaakov and D. Adar, "Averaged Models as Tools for Studying the Dynamics of Switch Mode DC-DC Converters," in Proc. IEEE PESC '94, pp. 1369-1376, June 1994.

[9] W. Ki, "Signal Flow Graph in Loop Gain Analysis of DC-DC PWM CCM Switching Converters," *IEEE Trans. Ckts. & Sys. I,* v. 45, n. 6, pp. 644-655, June 1998.

[10] K. Smedley and S. Ćuk, "Switching Flow-Graph Nonlinear Modeling Technique," *IEEE Trans. Power Electron.,* v. 9, n. 4, pp. 405-413, 1994.

[11] Y. Ma and K. Smedley, "Switching Flow-Graph Nonlinear Modeling Method for Multistate-Switching Converters," *IEEE Trans. Power Electron.,* v. 12, n. 5, pp. 854-861, Sept. 1997.

[12] M. Zhu and F. Luo, "Graphical Analytical Method for Power DC-DC Converters: Averaging Binary Tree Structure Representation," *IEEE Trans. Power Electron.,* v. 22, n. 2, pp. 701-705, March 2007.

[13] M. Veerachary, "Analysis of Fourth-Order DC-DC Converters: A Flow Graph Approach," *IEEE Trans. Ind. Electron.*, v. 55, n. 1, pp. 133-141, Jan. 2008.

[14] G.A. Rincón-Mora, *Analog IC Design with Low-Dropout Regulators,* New York: McGraw-Hill, 2009.